

Magic Wavelength for Atomic Motion Insensitive Optical Lattice Clocks

Hidetoshi Katori,^{1,2} Koji Hashiguchi,^{1,2} E. Yu. Il'inova,³ and V. D. Ovsiannikov³

¹*Department of Applied Physics, Graduate School of Engineering,
The University of Tokyo, Bunkyo-ku, Tokyo 113-8656, Japan*

²*CREST, Japan Science and Technology Agency,
4-1-8 Honcho Kawaguchi, Saitama 332-0012, Japan*

³*Physics Department, Voronezh State University, Universitetskaya pl.1, Voronezh 394006, Russia*

(Dated: November 5, 2018)

In a standing wave of light, a difference in spatial distributions of multipolar atom-field interactions may alter the definition of the magic wavelength to minimize the uncertainty of optical lattice clocks. We show that the magic wavelength can be determined so as to eliminate the spatial mismatch in electric dipole, magnetic dipole, and electric quadrupole interactions for specific combinations of standing waves. Experimental prospects of such lattices used with a blue magic wavelength are discussed.

PACS numbers: 37.10.Jk, 32.80.Qk, 32.80.Rm, 32.10.Dk, 06.30.Ft

Quantum absorbers trapped in well-designed electromagnetic fields are the excellent candidates for future optical atomic clocks projecting uncertainties exceeding 10^{-18} [1, 2], which represent the state of the art of the precision spectroscopy [3, 4]. While these atom traps provide long interrogation time and the Lamb-Dicke confinement of atoms necessary for ultrahigh resolution spectroscopy, the relevant trapping fields impose an inherent fundamental limit on measurement uncertainties due to the atomic multipolar interactions with trapping fields [1, 5, 6, 7] and hyperpolarizability effects [2, 8]. It is of note that the detection and control [9, 10, 11] of the electric quadrupole interactions of ions with their trapping fields triggered an essential breakthrough for ion clocks operating on the $S - D$ clock transitions to achieve the the uncertainties of 10^{-15} and even below [3, 12].

Recently it was pointed out that the multipolar interactions of atoms with optical lattices may introduce spatial mismatch of the lattice potentials in the clock transition thus affecting optical lattice clocks' uncertainties at 10^{-16} [13]. This inferred the slight breakdown of the original concept of the magic wavelength that cancels out the quadratic light shift in the clock transitions [2]. In this Letter, we discuss strategies to minimize the light shift uncertainties in optical lattice clocks by considering the electric dipole (E1), magnetic dipole (M1), and electric quadrupole (E2) interactions of atoms in a standing wave. For specific lattice geometries, we show that the magic frequency ω_m of a lattice clock can be defined so as to eliminate spatial mismatch of the lattice potentials, which is accompanied by a spatially constant differential light shift $\delta\nu$. Consequently, optical lattice clocks free from atomic-motion-dependent clock shift are realized and the offset $\delta\nu$ can be evaluated down to 10^{-18} as a correction for the clock frequency. We discuss experimental prospects for the $^1S_0 - ^3P_0$ clock transition of Sr atoms. In particular, combined with a blue-detuned

magic wavelength [14], the proposed lattice geometry closely simulates the Paul trap employed in ion clocks [1], thus pushing lattice clocks' uncertainty towards the 10^{-18} regime.

Optical lattices consist of a spatially periodic light shift formed by an interference pattern of electromagnetic waves. The simplest configuration is a one-dimensional (1D) lattice with a standing wave of light having wave vectors $\pm\mathbf{k}$ and parallel electric fields $\mathbf{E}_{\pm\mathbf{k}}$ as shown in Fig. 1(a). The corresponding magnetic fields $\mathbf{B}_{\pm\mathbf{k}}$ are proportional to $(\pm\mathbf{k}) \times \mathbf{E}_{\pm\mathbf{k}}$. As a result, anti-nodes of the total electric field $\mathbf{E} = \mathbf{E}_{+\mathbf{k}} + \mathbf{E}_{-\mathbf{k}} = 2\mathbf{E}_{\pm\mathbf{k}}$ correspond to nodes of the magnetic field $\mathbf{B} = \mathbf{B}_{+\mathbf{k}} + \mathbf{B}_{-\mathbf{k}} = 0$, and their amplitudes are a quarter of the wavelength $\lambda = 2\pi/|\mathbf{k}|$ out of phase, introducing different spatial dependences for the E1 and M1 interactions. Moreover, as the E2 interaction is proportional to the electric field gradient, its spatial dependence also differs from that of E1. These different spatial dependences do not allow perfect cancellation of the quadratic light shift in the clock transitions [13]. However, by admitting a constant differential light shift offset, we will show that spatial mismatch of the light shift can be eliminated, therefore the atomic motion dependent clock shift, which is detrimental to atomic clocks, can be removed.

As there are hyperpolarizability effects [2, 8] that cannot be moderated by the magic wavelength, a blue detuned magic wavelength that confines atoms near the nodes of standing waves would be a promising choice, which will reduce the relevant uncertainties down to 2×10^{-19} [14]. Although the local electric field intensity for atoms is reduced, the E2 interaction, in turn, may severely affect the accuracy of a blue detuned lattice clock, as the electric field gradient can generally be maximum at the nodes of the standing wave. These blue detuned lattices can be realized using 3D lattice configuration [15]. Moreover, application of single-occupancy 3D lattices with red and blue magic wavelengths may

effectively suppress the collision shift [16].

We consider 3D optical lattices consisting of three mutually orthogonal standing waves, whose results are straightforwardly applicable to lower dimensional lattices. In particular, we derive spatial dependences $q_X(\mathbf{r})$ of the quadratic light shift with $X = \text{E1, M1, and E2}$ interactions. For generality, we assume different electric field amplitudes $E_\xi = \rho_\xi E_0$ of the three standing waves with equal wavelength λ and wave number $k=2\pi/\lambda$ and different polarization vectors \mathbf{p}_ξ and \mathbf{p}_ξ^b ($|\mathbf{p}_\xi|=|\mathbf{p}_\xi^b|=1$) for the forward and backward running waves, respectively, in the $\xi=x, y, z$ directions denoted by unit vectors \mathbf{e}_ξ :

$$\begin{aligned} \mathbf{E}_\xi(\xi, t) &= E_\xi [\mathbf{p}_\xi \cos(k\xi - \omega t) + \mathbf{p}_\xi^b \cos(k\xi + \omega t)] \\ &= E_\xi (\mathbf{p}_\xi^+ \cos k\xi \cos \omega t + \mathbf{p}_\xi^- \sin k\xi \sin \omega t), \end{aligned} \quad (1)$$

where we define $\mathbf{p}_\xi^\pm \equiv \mathbf{p}_\xi \pm \mathbf{p}_\xi^b$. The total electric field vector in this lattice is given by $\mathbf{E}(\mathbf{r}, t) = \sum_{\xi=x,y,z} \mathbf{E}_\xi(\xi, t)$.

The principal contribution to the lattice potential is given by the second-order quasienergy shift due to the electric dipole atom-field interaction determined by the Hamiltonian $\hat{V}_{\text{E1}}(\mathbf{r}, \mathbf{r}_e, t) = -\mathbf{d} \cdot \mathbf{E}(\mathbf{r}, t)$ [17],

$$\begin{aligned} U_{\text{E1}}(\mathbf{r}) &= -\langle\langle \psi | \hat{V}_{\text{E1}} \mathcal{G}(\mathbf{r}_e, t; \mathbf{r}'_e, t') \hat{V}_{\text{E1}} | \psi \rangle\rangle \\ &= -\frac{E_0^2}{2} \alpha_{\text{E1}}(\omega) q_{\text{E1}}(\mathbf{r}), \end{aligned} \quad (2)$$

where \mathbf{r}_e is the position vector of the outermost atomic electron relative to the atomic nucleus at \mathbf{r} , $\mathbf{d} = -\mathbf{r}_e$ is the electric dipole moment, and $\mathcal{G}(\mathbf{r}_e, t; \mathbf{r}'_e, t')$ is the quasienergy Green function of an atom. Here the atomic units are used, $e=m=\hbar=1$, where the speed of light is $c \approx 137$. The double angular brackets in Eq. (2) denote the

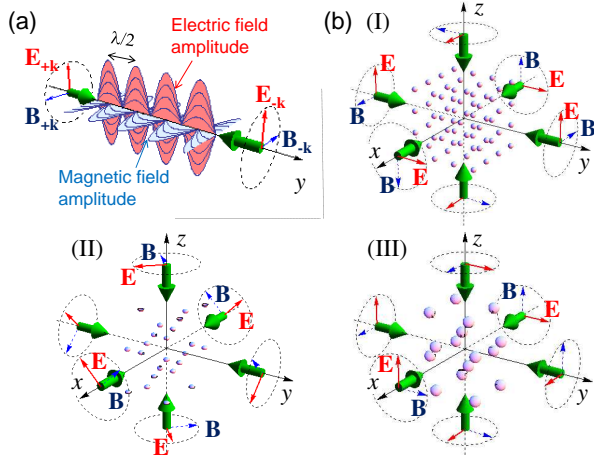


FIG. 1: (a) Spatial distribution of an electromagnetic field for a 1D standing wave. (b) Configuration of the electromagnetic fields and optical lattices for the cases (I)-(III), as described in the text. Optical lattice sites inside $|x|, |y|, |z| < 0.9\lambda$ are indicated with their equipotential surfaces given by $q_{\text{E1}}(\mathbf{r}) = 0.3$ and $\rho_\xi = 1$.

time integration (in variables t and t') over the field oscillation period $T=2\pi/\omega$ and the spatial integration over the position \mathbf{r}_e of the atomic electron. With the use of the electric field in Eq. (1), the spatial distribution function of the atom-field E1 interaction energy is given by

$$q_{\text{E1}}(\mathbf{r}) = \frac{1}{2} \left(\sum_{\xi} \rho_\xi \mathbf{p}_\xi^+ \cos k\xi \right)^2 + \frac{1}{2} \left(\sum_{\xi} \rho_\xi \mathbf{p}_\xi^- \sin k\xi \right)^2. \quad (3)$$

To evaluate the contribution of the M1 interaction, it is sufficient to determine the magnetic field component of the lattice, which for each running wave with wave vector \mathbf{k}_ξ is given by $\mathbf{B}_\xi(\mathbf{r}, t) = \mathbf{k}_\xi/k \times \mathbf{E}_\xi(\mathbf{r}, t)$. The total magnetic field corresponding to the electric field in Eq. (1) is given by,

$$\begin{aligned} \mathbf{B}(\mathbf{r}, t) &= \sum_{\xi=x,y,z} E_\xi (\mathbf{e}_\xi \times \mathbf{p}_\xi^+ \sin k\xi \sin \omega t \\ &\quad + \mathbf{e}_\xi \times \mathbf{p}_\xi^- \cos k\xi \cos \omega t). \end{aligned} \quad (4)$$

The magnetic dipole contribution to the lattice potential may be written similarly to Eq. (2), as the quasienergy shift corresponding to the atom-field M1 interaction is described by the Hamiltonian $\hat{V}_{\text{M1}} = -\hat{\mathbf{m}} \cdot \mathbf{B}(\mathbf{r}, t)$, where $\hat{\mathbf{m}} = -(\hat{\mathbf{J}} + \hat{\mathbf{S}})/2c$ is the magnetic moment of an atom with atomic total momentum \mathbf{J} and spin \mathbf{S} . The spatial distribution of the M1 interaction is given by,

$$\begin{aligned} q_{\text{M1}}(\mathbf{r}) &= \frac{1}{2} \left(\sum_{\xi} \rho_\xi \mathbf{e}_\xi \times \mathbf{p}_\xi^+ \sin k\xi \right)^2 \\ &\quad + \frac{1}{2} \left(\sum_{\xi} \rho_\xi \mathbf{e}_\xi \times \mathbf{p}_\xi^- \cos k\xi \right)^2. \end{aligned} \quad (5)$$

In the nonrelativistic approximation, the magnetic dipole polarizability in the n^1S_0 ground state is zero, while for the n^3P_0 metastable state, it is given by

$$\alpha_{\text{M1}}(\omega) = \frac{E_n^3P_1 - E_n^3P_0}{6c^2[(E_n^3P_1 - E_n^3P_0)^2 - \omega^2]}, \quad (6)$$

which is evidently the value of the second order in the fine-structure constant $\alpha=1/c$. $\alpha_{\text{M1}}(\omega)$ remains negative for ω higher than the $n^3P_0 - n^3P_1$ transition frequency.

Not less important than the M1 Stark shift may be the contribution of the electric quadrupole (E2) interaction,

$$\begin{aligned} U_{\text{E2}}(\mathbf{r}) &= -\langle\langle \psi | \hat{V}_{\text{E2}} \mathcal{G}(\mathbf{r}_e, t; \mathbf{r}'_e, t') \hat{V}_{\text{E2}} | \psi \rangle\rangle \\ &= -\frac{E_0^2}{2} \alpha_{\text{E2}}(\omega) q_{\text{E2}}(\mathbf{r}). \end{aligned} \quad (7)$$

The value of the quadrupole polarizability $\alpha_{\text{E2}}(\omega)$ is of the second order in the fine-structure constant α , just as the magnetic dipole polarizability in Eq. (6) is. The E2 interaction operator may be taken from the Taylor series in powers of the small parameter $k|\mathbf{r}_e| \ll 1$ for the total atom-electric-field interaction Hamiltonian,

$$\hat{V}_{\text{E}}(\mathbf{r}, \mathbf{r}_e, t) = \mathbf{r}_e \cdot \sum_{s=0}^{\infty} \frac{(\mathbf{r}_e \cdot \nabla)^s}{(s+1)!} \mathbf{E}(\mathbf{r}, t), \quad (8)$$

where all derivatives are taken with respect to the components of the position vector \mathbf{r} , while \mathbf{r}_e is assumed to be constant. $\hat{V}_E(\mathbf{r}, \mathbf{r}_e, t)$ includes all higher-order multipole interactions: The $s=0$ term corresponds to the Hamiltonian $\hat{V}_{E1}(\mathbf{r}, t)$ and the $s=1$ term to the Hamiltonian $\hat{V}_{E2}(\mathbf{r}, t)$. After substitution of this operator into Eq. (7) and integration over time and angular variables, the spatial distribution of the quadrupole energy is determined:

$$q_{E2}(\mathbf{r}) = \frac{1}{2} \sum_{(\xi, \eta)} \left(\rho_\xi \mathbf{e}_\eta \cdot \mathbf{p}_\xi^+ \sin k\xi + \rho_\eta \mathbf{e}_\xi \cdot \mathbf{p}_\eta^+ \sin k\eta \right)^2 + \frac{1}{2} \sum_{(\xi, \eta)} \left(\rho_\xi \mathbf{e}_\eta \cdot \mathbf{p}_\xi^- \cos k\xi + \rho_\eta \mathbf{e}_\xi \cdot \mathbf{p}_\eta^- \cos k\eta \right)^2, \quad (9)$$

where the sum runs over $(\xi, \eta) = (x, y), (y, z),$ and (z, x) . Correspondingly, the quadrupole polarizabilities of the ground and excited states are written in terms of the radial matrix elements, e.g., for the $|\psi\rangle = |n^1S_0\rangle$ state,

$$\alpha_{E2}^{1S_0}(\omega) = \frac{\omega^2}{60c^2} \langle n^1S_0 | r_e^2 (g_{1D_2}^\omega + g_{1D_2}^{-\omega}) r_e^2 | n^1S_0 \rangle, \quad (10)$$

where the radial Green functions $g_{1D_2}^{\pm\omega}$ of the singlet D -state subspace appear.

Below we illustrate a few representative examples that allow cancellation of spatial mismatch of the lattice potentials. They are assorted by the electric field \mathbf{E}_f and \mathbf{E}_b of the forward and backward running waves that compose lattice standing waves, as summarized in Fig. 1(b).

(I) $\mathbf{E}_f \parallel \mathbf{E}_b$ standing waves ($\mathbf{p}_\xi = \mathbf{p}_\xi^b$), in which we take $\mathbf{p}_x = \mathbf{e}_y$, $\mathbf{p}_y = \mathbf{e}_z$, and $\mathbf{p}_z = \mathbf{e}_x$. The E1 distribution is calculated to be,

$$q_{E1}(\mathbf{r}) = 2(\rho_x^2 \cos^2 kx + \rho_y^2 \cos^2 ky + \rho_z^2 \cos^2 kz). \quad (11)$$

The M1 and E2 distributions are given by,

$$q_{M1}(\mathbf{r}) = q_{E2}(\mathbf{r}) = \Delta q - q_{E1}(\mathbf{r}), \quad (12)$$

with $\Delta q = 2(\rho_x^2 + \rho_y^2 + \rho_z^2)$. Thus the distributions of M1 and E2 shifts in this lattice coincide and differ from $q_{E1}(\mathbf{r})$ in sign and by a constant offset of Δq .

(II) $\mathbf{E}_f \perp \mathbf{E}_b$ standing waves ($\mathbf{p}_\xi \perp \mathbf{p}_\xi^b$) with their polarization vectors pointing at an angle $\pi/4$ to the standing-wave beams, i.e., $\mathbf{p}_x = (\mathbf{e}_y + \mathbf{e}_z)/\sqrt{2}$, $\mathbf{p}_x^b = (-\mathbf{e}_y + \mathbf{e}_z)/\sqrt{2}$, $\mathbf{p}_y = (\mathbf{e}_z + \mathbf{e}_x)/\sqrt{2}$, $\mathbf{p}_y^b = (-\mathbf{e}_z + \mathbf{e}_x)/\sqrt{2}$, $\mathbf{p}_z = (\mathbf{e}_x + \mathbf{e}_y)/\sqrt{2}$ and $\mathbf{p}_z^b = (\mathbf{e}_x - \mathbf{e}_y)/\sqrt{2}$. The E1 and E2 distributions here coincide and M1 differs from them by sign and an offset,

$$q_{E1}(\mathbf{r}) = q_{E2}(\mathbf{r}) = \Delta q/2 + 2\rho_x\rho_z \sin kx \sin kz + 2\rho_y\rho_z \cos ky \cos kz, \quad (13)$$

$$q_{M1}(\mathbf{r}) = \Delta q - q_{E1}(\mathbf{r}).$$

(III) $\mathbf{E}_f \perp \mathbf{E}_b$ standing waves ($\mathbf{p}_\xi \perp \mathbf{p}_\xi^b$), in which we take polarization vectors to be $\mathbf{p}_x^\pm = \mathbf{e}_y \pm \mathbf{e}_z$, $\mathbf{p}_y^\pm = \mathbf{e}_z \pm \mathbf{e}_x$, and

$\mathbf{p}_z^\pm = \mathbf{e}_x \pm \mathbf{e}_y$. Then the E1 and M1 distributions coincide and E2 differs from them by sign and an offset,

$$q_{E1}(\mathbf{r}) = q_{M1}(\mathbf{r}) = \Delta q/2 + \rho_x\rho_y \cos k(x+y) + \rho_y\rho_z \cos k(y+z) + \rho_z\rho_x \cos k(z+x), \quad (14)$$

$$q_{E2}(\mathbf{r}) = \Delta q - q_{E1}(\mathbf{r}).$$

As indicated by these examples, it is essential that the spatial distributions of $q_X(\mathbf{r})$ may show the same spatial dependences apart from the sign and an offset Δq for particular lattice geometries. However, we note that this is not a general feature for optical lattices. For example, in the 3D lattice with $\mathbf{E}_f \parallel \mathbf{E}_b$ standing waves with $\mathbf{p}_x = \mathbf{p}_y = \mathbf{e}_z$ and $\mathbf{p}_z = \mathbf{e}_x$ employed in our previous experiment [16], neither $q_{M1}(\mathbf{r})$ nor $q_{E2}(\mathbf{r})$ shows the same spatial dependences as $q_{E1}(\mathbf{r})$, therefore the motional effects may limit clock uncertainties in future experiments.

These three examples show prominent features by themselves. For a magic frequency, where the E2 (M1) interaction is significantly larger than the M1 (E2) interaction, case (II) [case (III)] will be more advantageous than the others, as the less significant M1 (E2) contribution may well be neglected. For application to the blue magic wavelength, which highlights the reduction of the hyperpolarizability effects by trapping atoms near the nodes, case (I) would be a reasonable choice, as Eq. (11) suggests the creation of perfect nodes regardless of the intensity balance in the orthogonal lattice beams. Regarding the lattice light polarization, case (I) shows linear polarization, while cases (II) and (III) have elliptical polarizations that may give rise to the vector shift for atoms with non-zero angular momentum.

Hereafter, we focus on case (I) and consider its application to the blue detuned magic wavelength. The clock transition frequency is expressed as

$$\nu_{\text{clock}}(\omega) = \nu_0 - \frac{1}{2} \Delta\alpha_{EM}(\omega) q_{E1}(\mathbf{r}) E_0^2 - \frac{1}{2} \Delta\alpha_0(\omega) \Delta q E_0^2 + \mathcal{O}(E_0^4), \quad (15)$$

where ν_0 is the atomic transition frequency, ω is the lattice laser frequency. The quadratic light shift is decomposed into two parts depending on their spatial dependences by $\Delta\alpha_{EM}(\omega) \equiv \Delta\alpha_{E1}(\omega) - \Delta\alpha_{M1}(\omega) - \Delta\alpha_{E2}(\omega)$ and $\Delta\alpha_0(\omega) \equiv \Delta\alpha_{M1}(\omega) + \Delta\alpha_{E2}(\omega)$ using differential E1, M1, and E2 polarizabilities in the clock transition. Besides the hyperpolarizability effects that are minimized by use of a blue-detuned lattice [14], the magic frequency ω_m may be given by $\Delta\alpha_{EM}(\omega_m) = 0$, allowing us to define ω_m independent of atomic motional states. The residual M1-E2 term $\delta\nu = -\frac{1}{2} \Delta\alpha_0(\omega_m) \Delta q E_0^2$ provides an atomic-position-independent offset, which is solely related to the total lattice laser intensity $\Delta q E_0^2 = 2(E_x^2 + E_y^2 + E_z^2)$.

To find the magic frequency, it is essential to extract the atomic-motion-dependent term in Eq. (15). Harmonically approximating the trapping potential near the lattice node at $x=y=z=\lambda/4$ and averaging over the atom

positions in the oscillator state $|\mathbf{n}\rangle = |n_x, n_y, n_z\rangle$, the second term in the right-hand side of Eq. (15) should be replaced with

$$2 \left\langle -\frac{1}{2} \Delta \alpha_{\text{EM}} q_{\text{E1}}(\mathbf{r}) E_0^2 \right\rangle_{\mathbf{n}} = \sum_{\xi} (\Omega_{\xi}^P - \Omega_{\xi}^S) (n_{\xi} + \frac{1}{2}), \quad (16)$$

where $\Omega_{\xi}^{(\ell)} = k \rho_{\xi} E_0 \sqrt{2|\alpha_{\text{EM}}^{(\ell)}(\omega)|/\mathcal{M}}$ is the vibrational frequency of atoms in the ξ direction of the lattice potential for the $\ell = P(^3P_0)$ or $S(^1S_0)$ state. Here \mathcal{M} is the mass of the atom, $\alpha_{\text{EM}}^{(\ell)}(\omega) \equiv \alpha_{\text{E1}}^{(\ell)}(\omega) - \alpha_{\text{M1}}^{(\ell)}(\omega) - \alpha_{\text{E2}}^{(\ell)}(\omega)$ is given by the E1, M1, and E2 polarizabilities in the ℓ state, and factor 2 accounts for the kinetic energy.

Atomic-motion-dependent effects can be identified by the clock frequency difference $\Delta\nu(\omega, \delta\mathbf{n}) = \nu_{\text{clock}}(\omega, \delta\mathbf{n} + \mathbf{n}) - \nu_{\text{clock}}(\omega, \mathbf{n})$ measured for atoms occupying vibrational states differing by $\delta\mathbf{n}$. The magic frequency ω_m [19] can be determined by $\Delta\nu(\omega_m, \delta\mathbf{n}) = 0$, equivalent to $\Delta\alpha_{\text{EM}}(\omega_m) = \alpha_{\text{EM}}^P(\omega_m) - \alpha_{\text{EM}}^S(\omega_m) = 0$. Once the magic frequency is determined, the residual M1-E2 offset $\delta\nu$ can be evaluated in terms of the vibrational frequencies of the lattice potential $\Omega_{\xi} = \Omega_{\xi}^S(\omega_m) = \Omega_{\xi}^P(\omega_m)$ as

$$\delta\nu = -\frac{\mathcal{M}\Delta\alpha_0}{2k^2|\alpha_{\text{EM}}|} (\Omega_x^2 + \Omega_y^2 + \Omega_z^2). \quad (17)$$

Therefore all the essential measurements are done by the frequency measurements, once the magic frequency/wavelength is measured and shared. The same strategy should apply to 1D optical lattices with red-detuned magic wavelength by setting $\rho_x \neq 0$ and $\rho_y = \rho_z = 0$ in case (I).

The proposed optical lattice will be conveniently realized by a folded lattice [16, 18], which maintains the relative phases of the orthogonal standing waves to realize linear lattice polarizations. Eq. (1) essentially assumes that the intensities of the counter-propagating beam pairs are balanced, which is accomplished by preparing lattice beams inside an optical cavity [16]. The blue-detuned magic wavelength for the Sr clock transition is experimentally determined to be $\lambda_m = 2\pi c/\omega_m \approx 389.9$ nm [14], where the numerical estimates for this lattice give $\Delta\alpha_0/|\alpha_{\text{EM}}| \approx -1.4 \cdot 10^{-7}$ with $\Delta\alpha_{\text{M1}}/\Delta\alpha_{\text{E2}} \approx 8 \cdot 10^{-3}$ [20]. Therefore, the offset frequency is given by $\delta\nu/2\pi \approx 40 \cdot I$ mHz for a trap frequency of $\Omega_{\xi}/2\pi = 75\sqrt{I}$ kHz, where I is the single running wave laser intensity measured in kW/cm² assuming $\rho_{\xi} = 1$. The uncertainty for this correction may be evaluated to be $\approx 4I$ mHz, assuming an inhomogeneity of the lattice intensity of 10 %.

For ⁸⁷Sr atoms with a total angular momentum of $F=9/2$, the tensor light shift due to the spatial rotation of the lattice polarization with respect to the quantization axis may occur. As the shift is proportional to the light intensity near the nodes, the shift may be reduced to the mHz level for the blue magic wavelength. Bosonic

isotopes such as ⁸⁸Sr or other atomic elements with nuclear spin of $I=1/2$, e.g., ¹⁷¹Yb or ¹⁹⁹Hg may well be used to suppress the tensor light shift.

In summary, we present general formulae for the quadratic light shift taking multipolar atom-field interactions into account and show that the spatial mismatch of the interactions in the clock transition can be treated as a spatially constant offset $\delta\nu$ for specific lattice geometries. Numerical estimates are made for Sr atoms, and the relevant correction can be determined by trap frequency measurements with the mHz level. Combined with the blue magic wavelength, the hyperpolarizability effect is minimized, and clock uncertainty at the 10^{-18} level will be within reach.

This work was partly supported by the Photon Frontier Network Program, MEXT, Japan, and by the Russian Foundation for Basic Research (RFBR grant No. 07-02-00279a). H. K. acknowledges M. Takamoto for useful comments.

-
- [1] H. G. Dehmelt, IEEE Trans. Instrum. Meas. **IM-31**, 83 (1982).
 - [2] H. Katori, M. Takamoto, V. G. Pal'chikov, and V. D. Ovsiannikov, Phys. Rev. Lett. **91**, 173005 (2003).
 - [3] T. Rosenband et al., Science **319**, 1808 (2008).
 - [4] A. D. Ludlow et al., Science **319**, 1805 (2008).
 - [5] N. Yu, X. Zhao, H. Dehmelt, and W. Nagourney, Phys. Rev. A **50**, 2738 (1994).
 - [6] W. M. Itano, J. Res. Natl. Inst. Stand. Technol **105**, 829 (2000).
 - [7] A. V. Taichenachev et al., Phys. Rev. Lett. **96**, 083001 (2006).
 - [8] A. Brusch, R. Le Targat, X. Baillard, M. Fouch, and P. Lemonde, Phys. Rev. Lett. **96**, 103003 (2006).
 - [9] G. P. Barwood, H. S. Margolis, G. Huang, P. Gill, and H. A. Klein, Phys. Rev. Lett. **93**, 133001 (2004).
 - [10] P. Dubé et al., Phys. Rev. Lett. **95**, 033001 (2005).
 - [11] C. F. Roos, M. Chwalla, K. Kim, M. Riebe, and R. Blatt, Nature **443**, 316 (2006).
 - [12] T. Schneider, E. Peik, and C. Tamm, Phys. Rev. Lett. **94**, 230801 (2005).
 - [13] A. V. Taichenachev, V. I. Yudin, V. D. Ovsiannikov, V. G. Pal'chikov, and C. W. Oates, Phys. Rev. Lett. **101**, 193601 (2008).
 - [14] M. Takamoto, H. Katori, S. I. Marmo, V. D. Ovsiannikov, and V. G. Pal'chikov, Phys. Rev. Lett. **102**, 063002 (2009).
 - [15] Mueller-Seydlitz et al., Phys. Rev. Lett. **78**, 1038 (1997).
 - [16] T. Akatsuka, M. Takamoto, and H. Katori, Nat. Phys. **4**, 954 (2008).
 - [17] N. L. Manakov, V. D. Ovsiannikov, and L. P. Rapoport, Physics Reports **141**, 320 (1986).
 - [18] A. Rauschenbeutel, H. Schadwinkel, V. Gomer, and D. Meschede, Opt. Commun. **148**, 45 (1998).
 - [19] This definition of the magic frequency is different from that in Ref. [14] determined for a traveling wave.
 - [20] As for the red-detuned lattice at $\lambda_m \approx 813.4$ nm, $\Delta\alpha_0/|\alpha_{\text{EM}}| \approx -3.3 \cdot 10^{-8}$ with $\Delta\alpha_{\text{M1}}/\Delta\alpha_{\text{E2}} \approx 7 \cdot 10^{-2}$.